Receptors, sparks and waves in a fire-diffuse-fire framework for calcium release

S Coombes[†] and R Hinch[‡] and Y Timofeeva[*]

[†] *Centre for Mathematical Medicine, School of Mathematical Sciences, University of Nottingham, Nottingham, NG7 2RD, UK.*

[‡] *Centre for Mathematical Biology, Mathematical Institute, University of Oxford, 24-29 St Giles', Oxford, OX1 3LB, UK.*

[*] *Mathematical Biology Group, Department of Mathematical Sciences, Loughborough University, Loughborough, Leicestershire, LE11 3TU, UK.*

Preprint submitted to Elsevier Science *23 January 2004*

Abstract

Calcium ions are an important second messenger in living cells. Indeed calcium signals in the form of waves have been the subject of much recent experimental interest. It is now well established that these waves are composed of elementary stochastic release events (calcium puffs or sparks) from spatially localised calcium stores. The aim of this paper is to analyse how the stochastic nature of individual receptors within these stores combines to create stochastic behaviour on long timescales that may ultimately lead to waves of activity in a spatially extended cell model. Techniques from asymptotic analysis and stochastic phase-plane analysis are used to show that a large cluster of receptor channels leads to a release probability with a sigmoidal dependence on calcium density. This release probability is incorporated into a computationally inexpensive model of calcium release based upon a stochastic generalization of the Fire-Diffuse-Fire (FDF) threshold model. Numerical simulations of the model in one and two dimensions (with stores arranged on both regular and disordered lattices) illustrate that stochastic calcium release leads to the spontaneous production of calcium sparks that may merge to form saltatory waves. Illustrations of spreading circular waves, spirals and more irregular waves are presented. Furthermore, receptor noise is shown to generate a form of array enhanced coherence resonance whereby all calcium stores release periodically and simultaneously.

Key words: calcium sparks, ryanodine receptors, intracellular signalling, fire-diffuse-fire, stochastic transitions, calcium waves

1 Introduction

Ca^{2+} is critically important for a large number of cellular functions, such as muscle contraction, cardiac electrophysiology, bursting oscillations and secretion (in response to hormonal agonists or neurotransmitters), synaptic plasticity, sensory perception and adaptation in photoreceptors (Berridge, 1997). Ca^{2+} signalling in a wide diversity of cell types frequently occurs as repetitive, but transient, increases in $[Ca^{2+}]$ or Ca^{2+} oscillations. The changes in $[Ca^{2+}]$ associated with Ca^{2+} oscillations generally do not occur uniformly throughout the cell but are initiated at a specific site and spread in the form of waves. The functional significance of these spatio-temporal patterns of $[Ca^{2+}]$ is a subject of increasing activity within the cellular signalling community. For example, in the spatial domain the spreading of a Ca^{2+} wave provides a mechanism by which a regulatory signal can be distributed throughout the cell (Callamaras et al., 1998). Two classes of oscillations or waves are readily distinguished: those that depend primarily on the influx of Ca^{2+} through voltage-operated Ca^{2+} channels (VOCCs) from the extracellular space, and those that depend primarily on Ca^{2+} release from internal stores. In this latter class, distinctions can be made on the basis of whether the release of Ca^{2+} is dominated by the ryanodine receptor (RyR), the inositol (1,4,5)-trisphosphate (IP_3) receptor or a combination of both. When activated, both Ca^{2+} entry and Ca^{2+} release channels can give rise to brief pulses of Ca^{2+} that form a small plume around the mouth of the channel before diffusing into the cytoplasm. One type of local Ca^{2+} signal that appears to operate in many electrically non-excitable cells is Ca^{2+} *puffs*. These elementary events have amplitudes typically ranging from $\sim 50-600$nM, a spatial spread of $\sim 6\mu$m and a total duration of ~ 1 second. Such events were first observed in Xenopus oocytes (Yao et al., 1995) but have subsequently been observed in HeLa cells, neurites and endothelial cells (reviewed in (Bootman et al., 2001)). It is now well established that cell-specific recruitment of a generic elementary signal underlies different global signals. In heart and skeletal muscle, release of Ca^{2+} from the sarcoplasmic reticulum (SR) by RyRs is the key event linking membrane depolarisation and mechanical activity during excitation-contraction coupling. RyRs occur in clusters that give rise to localised Ca^{2+}-release events denoted Ca^{2+} *sparks* (Cheng et al., 1993). These events are analogous to the Ca^{2+} puffs described above, although they are usually faster in onset and decline, and have a more restricted spread ($\sim 1-3\mu$m). Spatio-temporal recruitment of Ca^{2+} sparks underlies the global Ca^{2+} signals that subsequently activate myocyte contraction (Stern, 1992).

Ca^{2+} sparks and puffs are simple examples of the stochastic nature of intracellular Ca^{2+} dynamics. The timescale on which stochasticity is observed when puffs or sparks are triggered is of the order of many seconds. However, the origin of the stochastic nature of Ca^{2+} release events lies in the individual gating of Ca^{2+}-channels, which occur on the millisecond timescale. One question we aim to address in this paper is how stochastic behaviour at a short timescale is able to induce stochastic effects on a much longer timescale. This 'jumping' of timescales occurs because the Ca^{2+}-channels are arranged in localised clusters of 10–100 receptors.

In brief, the fluorescent imaging of localised Ca^{2+} puffs or sparks has now made it clear that Ca^{2+} release is a stochastic process that occurs at spatially discrete sites that are clusters of IP_3 receptors in the endoplasmic reticulum (ER) or RyRs in the SR. The amount of Ca^{2+} released, in response to a triggering event, can be considerably greater than the initial flux of Ca^{2+}, but only if this initial flux exceeds some threshold (Callamaras et al., 1998). This is an example of a nonlinear feedback process, often referred to as Ca^{2+}-induced Ca^{2+} release (CICR). For example, in skeletal muscle, an initial SR Ca^{2+} release is governed by voltage-sensors but subsequently activates additional Ca^{2+} sparks by CICR release from the SR. CICR is believed to be the major mechanism underlying wave propagation via diffusion of locally released Ca^{2+} to neighbouring release sites, causing neighbouring channels to open and release more Ca^{2+} (Allbritton and Meyer, 1993). Typically the autocatalytic release of Ca^{2+} terminates once $[Ca^{2+}]$ reaches a sufficiently high level. Beyond this level processes which take up Ca^{2+} from the cytosol dominate the dynamics. These involve transport of Ca^{2+} into the extracellular medium and into the ER or SR by exchangers and pumps located in the cell membranes.

Some example of experimental linescan images from a ventricular myocyte showing sparks, waves and partial waves are shown in Figure 1. Importantly, high-resolution imaging of Ca^{2+} in a variety of cell types shows that travelling waves in living cells can vary in their appearance. For example, the calcium wave that occurs during fertilization in mature *Xenopus* eggs appears to be continuous (Fontanilla and Nuccitelli, 1998; Nuccitelli et al., 1993), whereas the calcium wave in immature *Xenopus* oocytes propagates as a sequence of bursts (Callamaras et al., 1998; Parker and Yao, 1991; Parker et al., 1996; Yao et al., 1995).

Although theoretical work on Ca^{2+} dynamics has increased in recent years (reviewed in (Sneyd, 2002)), the spatially extended nature of the cell combined with the stochastic

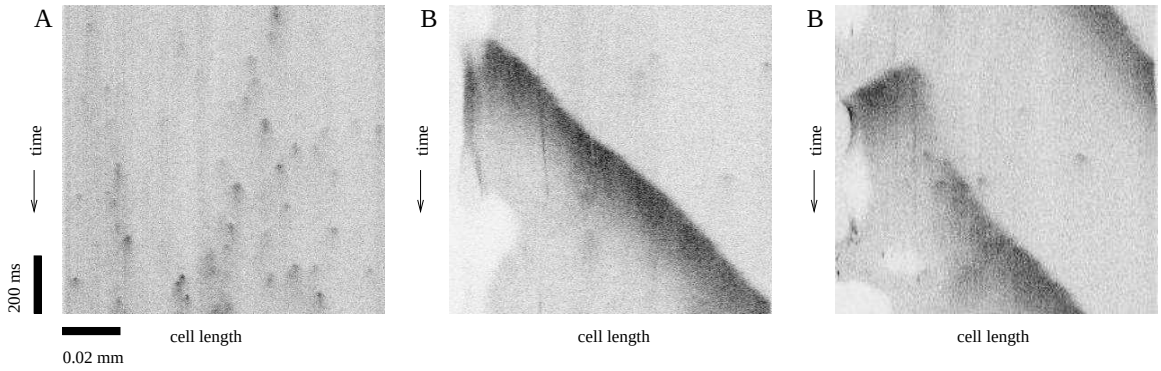

Fig. 1. Linescan images of an isolated rat ventricular myocyte (with elevated intracellular $[Ca^{2+}]$) exhibiting (A) Ca^{2+} sparks; (B) a Ca^{2+} wave; and (C) a Ca^{2+} wave which fail to propagate the length of the cell (light = low $[Ca^{2+}]$ and dark = high $[Ca^{2+}]$). Ca^{2+} oscillations were induced by increasing intracellular $[Ca^{2+}]$ using oubain. The Ca^{2+} was imaged using the fluorescent indicator fluo-3 and confocal microscopy. The linescan shows a cell length of 100 μm sampled every 2 ms for 1 s.

nature of localised calcium release and the heterogeneous distribution of Ca^{2+} stores has received far less attention. Recently, however, Coombes and Timofeeva have developed a mathematical framework to address these issues (Timofeeva and Coombes, 2003; Coombes and Timofeeva, 2003). This work builds upon the earlier theoretical work of Keizer and Smith (1998) and Falcke et al. (2000), who were the first to stress the importance of noise in the generation of spark to wave transitions and its role in generating slow pacemaker oscillations. The first prototype model developed in our framework is equivalent to a stochastic generalisation of the deterministic Fire-Diffuse-Fire (FDF) model of Keizer et al. (1998). The latter is a model of cardiac myocytes in which calcium release occurs via RyRs located in a regular array in the SR. FDF models use a threshold process to mimic the nonlinear properties of Ca^{2+} channels. The stochastic nature of release is incorporated via the introduction of a simple probabilistic rule for the release of calcium from internal stores. By avoiding a Markov process description of channel gating we sidestep the need for computationally expensive Monte Carlo type simulations. Moreover, the simplicity of the underlying deterministic FDF model can lead to further computational improvements. When considering a discrete set of release sites and calcium puffs that have a simple on/off temporal structure the calcium profile can be solved for in closed form. This obviates the need to numerically evolve a partial differential equation to obtain calcium profiles (at least for diffusive transport).

In this review paper we describe how stochastic phase-plane analysis may be used to

analyse stochastic transitions in models of Ca^{2+} release units. Making use of mathematical techniques from asymptotic analysis gives a Markov chain with slowly varying coefficients that can be analysed to determine calcium release probability for a given receptor model. When incorporated within a generalised FDF framework we show how this is a natural way to investigate spark to wave transitions within a spatially extended cell model with a discrete distribution of release sites.

2 Analysis of calcium sparks

In this section we model Ca^{2+} release from a localised cluster of receptors in a Ca^{2+} release unit (CaRU). The aim is to examine how the stochastic gating of individual receptors in the cluster, which (assuming a cluster of 50 receptors) occur on a time scale of the order of 0.02 ms, affects the dynamics of the whole CaRU on time scales of 10–10^6 ms. This is achieved mathematically using an asymptotic analysis which allows us to approximate the ensemble behaviour of the whole cluster in the limit that it contains a large number of receptors. The asymptotic analysis also takes advantage of the fact that certain biophysical processes occur on different timescales. The model we present was originally developed for cardiac myocytes (Hinch, 2002, 2004) but is also applicable to local Ca^{2+} release in other cells.

We now briefly describe the biophysical mechanisms included in the Ca^{2+}-spark model, a detailed derivation can be found in Hinch (2004) . Figure 2 shows a schematic diagram of a CaRU in a cardiac myocyte. A cardiac myocyte contains approximately 10,000 CaRUs,

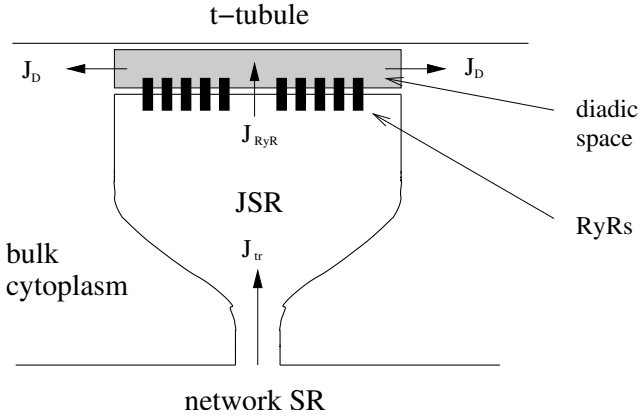

Fig. 2. The components of a CaRU which are situated at localised points in the cell where the SR is close to the t-tubules.

and each CaRU contains between $N \approx 10 - 100$ RyRs. Ca^{2+} is released from the SR

through the RyRs into a small region (the diadic space) between the SR and t-tubules. Define $[Ca^{2+}]_{ds}$ as the $[Ca^{2+}]$ in the diadic space, $[Ca^{2+}]_{myo}$ as the $[Ca^{2+}]$ in the bulk myoplasm, J_{RyR} as the current through the RyRs into the diadic space, and J_D as the diffusive current from the space into the bulk myoplasm. The diffusive current is simply modelled by

$$J_D = g_D([Ca^{2+}]_{ds} - [Ca^{2+}]_{myo}), \tag{1}$$

where g_D is the conductance. The flux balance equation for Ca^{2+} in the diadic space is

$$V_{ds}\frac{d[Ca^{2+}]_{ds}}{dt} = J_{RyR} - g_D([Ca^{2+}]_{ds} - [Ca^{2+}]_{myo}), \tag{2}$$

where V_{ds} is the volume of the diadic space. The mean open time of each RyR is τ_{open} and is the timescale over which J_{RyR} varies. Using experimental estimates for the parameters, $V_{ds}/g_D\tau_{open} \approx 0.002 \ll 1$, so the steady-state approximation for $[Ca^{2+}]_{ds}$ can be used

$$[Ca^{2+}]_{ds} \sim [Ca^{2+}]_{myo} + \frac{J_{RyR}}{g_D}. \tag{3}$$

In words this equation states that the $[Ca^{2+}]$ in the diadic space is equal to the $[Ca^{2+}]$ in the bulk myoplasm plus a quantity proportional to the current into the diadic space. Therefore when Ca^{2+} is released from the SR, the $[Ca^{2+}]$ in the diadic space is higher than in the bulk myoplasm. Only Ca^{2+} in the junctional-SR (JSR) can be released immediately by the RyRs, and the Ca^{2+} in the network-SR (NSR) must diffuse into the JSR before it can be released. Ca^{2+} is buffered in both the myoplasm (e. g. by calmodulin) and in the SR (e. g. by calsequestrin). The flux balance equation for Ca^{2+} in the JSR is

$$\frac{d[Ca^{2+}]_{JSR}}{dt} = \beta_{JSR}\left(-\frac{J_{RyR}}{V_{JSR}} - \frac{[Ca^{2+}]_{NSR} - [Ca^{2+}]_{JSR}}{\tau_{tr}}\right), \tag{4}$$

where $[Ca^{2+}]_{JSR}$ and $[Ca^{2+}]_{NSR}$ are the $[Ca^{2+}]$ in the JSR and NSR respectively, V_{JSR} is the volume of the JSR, β_{JSR} is the buffering factor, and τ_{tr} is the time constant of transfer of Ca^{2+} from the NSR to JSR. Define n as the number of RyRs open and $\phi = n/N$ as the proportion of the RyR in the cluster open. The total current through the RyRs is given by

$$J_{RyR} = J_R\phi([Ca^{2+}]_{JSR} - [Ca^{2+}]_{ds}) \tag{5}$$

Using the fact that $[Ca^{2+}]_{JSR} \gg [Ca^{2+}]_{ds}$, and combining (3) and (5), tells us that the $[Ca^{2+}]_{ds}$ is only a function of ϕ and $[Ca^{2+}]_{JSR}$. Using experimental estimates for the parameters (Hinch, 2004), the ratio of the timescale of the depletion of the JSR to the

open probability of the RyRs is $\tau_{\mathrm{JSR}} = V_{\mathrm{JSR}}/J_R\beta_{\mathrm{JSR}}\tau_{\mathrm{open}} \approx 15 \gg 1$, therefore the rate of depletion of the JSR is slow compared with the timescale over which J_{RyR} varies. Individual RyRs display modal-gating (Zahradnikova and Zahradnik, 1996), where the receptors open and close rapidly (≈ 1 ms) according to a Markov process, and the proportion of time the receptor is in the open state depends on the mode. When Ca^{2+} binds to a RyR, the mode of the RyR changes from one where the receptor is always closed to one where it is mainly open. This feature of the RyR means that the CaRU displays positive feedback: as more RyRs open the Ca^{2+} current from the JSR increases, this in turn increase $[Ca^{2+}]_{\mathrm{ds}}$ thus opening more RyRs. The sensitivity of the RyRs to $[Ca^{2+}]_{\mathrm{ds}}$ depends on $[Ca^{2+}]_{\mathrm{JSR}}$ (Lukyanenko et al., 1998; Thedford et al., 1994; Sobie et al., 2002). The RyRs are inactivated by both Ca^{2+}-dependent (Gyorke and Fill, 1993) and time-dependent process (Zahradnikova and Zahradnik, 1996). However, experiments on isolated RyRs show that the time-scale on which this occurs is much longer than that of a spark, therefore RyR inactivation is not included in this model. A model of RyR displaying modal-gating can be simplified to a 2-state model containing one closed state and one open state (Hinch, 2004). The rate of channel openings is k_+ and the rate of channel closing is k_-:

$$k_+ = \frac{[Ca^{2+}]^{\alpha}_{\mathrm{ds}}}{k\tau_{\mathrm{open}}([Ca^{2+}]^{\alpha}_{\mathrm{ds}} + K^{\alpha}_{\mathrm{RyR}})} \quad \text{and} \quad k_- = \frac{1}{\tau_{\mathrm{open}}}, \tag{6}$$

where k is the proportion of time the channel is open in the high mode, α is the Hill coefficient for Ca^{2+} binding to the channel, and K_{RyR} is the dissociation constant of the RyR. K_{RyR} is modelled with a linearly decreasing function SR $[Ca^{2+}]$ (Sobie et al., 2002) which reflects the decrease in sensitivity of the RyR at reduced $[Ca^{2+}]_{\mathrm{JSR}}$ (Lukyanenko et al., 1998; Thedford et al., 1994). Note that since $[Ca^{2+}]_{\mathrm{ds}}$ is only a function of ϕ and $[Ca^{2+}]_{\mathrm{JSR}}$, the transition rates $k_\pm$ are also only a function of ϕ and $[Ca^{2+}]_{\mathrm{JSR}}$. This allows the model to be written as a Markov chain (for the number of RyRs open) with slowly varying coefficients (since $\tau_{\mathrm{JSR}} \gg 1$). The rate of transitions from the n to $n+1$ state is $f(\phi, J)$, and the rate of transitions from the n to $n-1$ state is $g(\phi)$, where

$$f(\phi, J) = \frac{N(1-\phi)(J\phi + \epsilon_{\mathrm{m}})^{\alpha}}{k((1-\delta J)^{\alpha} + (J\phi + \epsilon_{\mathrm{m}})^{\alpha})} \quad \text{and} \quad g(\phi) = N\phi. \tag{7}$$

All variables and parameters have been non-dimensionalised (see Hinch (2004) for details): J is $[Ca^{2+}]_{\mathrm{JSR}}$; ϵ_m is $[Ca^{2+}]_{\mathrm{myo}}$; δ is the sensitivity of Ca^{2+} binding to the RyR on $[Ca^{2+}]_{\mathrm{JSR}}$. The rate at which Ca^{2+} is depleted from the JSR during Ca^{2+} release is given

by

$$\tau_{\mathrm{JSR}}\frac{\mathrm{d}J}{\mathrm{d}t} = -J\phi + r(J_0 - J), \tag{8}$$

where τ_{JSR} is the time constant of depletion; J_0 is the $[\mathrm{Ca}^{2+}]_{\mathrm{NSR}}$; and r is the rate of refill of the JSR from the NSR. The coefficients of the Markov chain (7) are a function of J, which is slowly varying because $\tau_{\mathrm{JSR}} \gg 1$.

The first part of the analysis is to examine the behaviour of the Markov chain when J is constant, which is the case before a spark is triggered. Figure 3A shows the results of a sample Monte Carlo simulation of the chain. Note that the system remains for a large time in the region of ϕ_+ where most of the receptors are open (i. e. during a spark), before undergoing a rapid jump to $\phi = 0$. This is an example of *metastability*, where the system

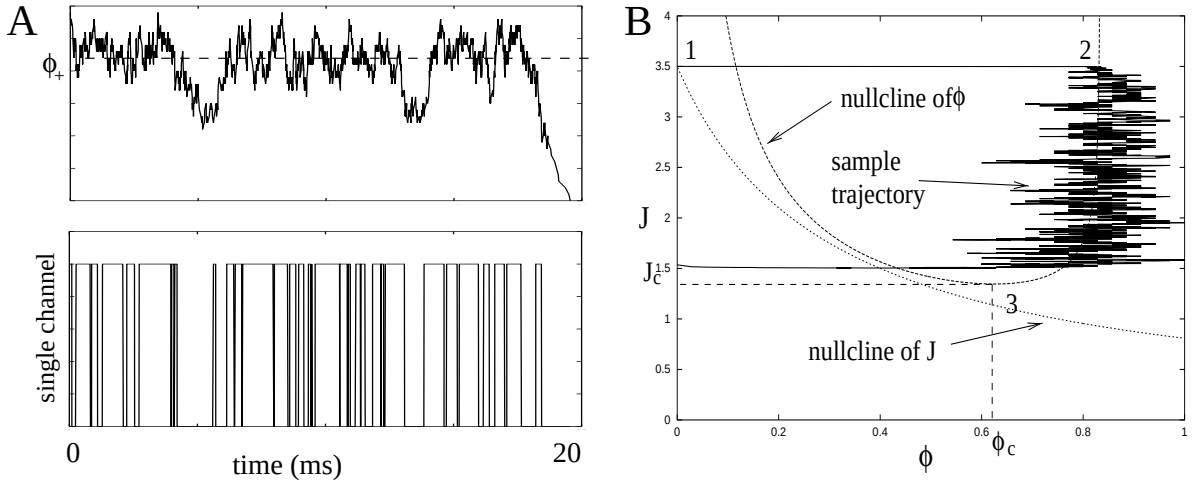

Fig. 3. A. A sample solution of the spark model. The upper trace is the proportion of all receptors which are open (ϕ). The lower trace is the opening of a single channel in the cluster. B. A sample solution in the phase–plane. At rest the system is at [1], when a spark is triggered it jumps to the null–cline ϕ_+ at [2]. It then moves down the null–cline, but is terminated by a stochastic transition before [3].

remains in the region of one stable fixed–point before for long periods making a rapid transition to another stable fixed–point. Metastability is the reason why stochasticity on the sub-millisecond time-scale can manifest itself on time-scales of many seconds. The fixed–points occur where $f(\phi_*) = g(\phi_*)$ and are stable if $g'(\phi_*) > f'(\phi_*)$. Note that between any two stable fixed–points there must be an unstable fixed point where $g'(\phi_*) < f'(\phi_*)$. When $[\mathrm{Ca}^{2+}]_{\mathrm{JSR}}$ is sufficiently high ($J > J_c$), the Markov chain (7) has two stable fixed points $\phi_\pm$ and one unstable fixed point ϕ_0. When analysing the properties of sparks, we are not interested in knowing the exact number of RyRs open, just whether

a spark is occurring or not (i. e. in the region of which stable fixed–point the system is). Therefore the quantity we are interested in is the mean first–passage time between the stable fixed–points. This can be calculated using an asymptotic analysis in the limit of a large number of RyRs in the CaRU ($N \nearrow \infty$). Define p_n as the probability that n receptors are open. The evolution of $p_n(t)$ is then described by the Master equation

$$\frac{\mathrm{d}p_n}{\mathrm{d}t} = f((n-1)/N)p_{n-1} - \Big(f(n/N) + g(n/N)\Big)p_n + g((n+1)/N)p_{n+1}, \tag{9}$$

and we remember that f and g are functions of $\phi = n/N$. The mean first–passage time can be calculated in a number of ways. For example, the steady–state solution for p_n can be calculated by approximately solving the detailed balance equation, and then analysing the behaviour of the chain in the region of the unstable fixed–point to obtain the mean first–passage time (Hinch, 2004). Alternatively the mean first–passage time can be calculated using a Wentzel-Kramers-Brillouin (WKB) approximation technique (and will be presented in detail elsewhere). The WKB ansatz is applied directly to the Master equation and the limit of large N is taken (note this approach is different to analysing the Fokker-Planck equation). In the WKB analysis the connection formulae at the turning points (which are at the fixed–points) fail to uniquely determine the steady–state solution. Calculating the solution at higher orders fails to remove this indeterminacy, which is due to the difference operator on the r.h.s. of (9) having an exponentially small eigenvalue (and hence the system displays metastability). Only once this exponentially small term is taken into account using the projection method (Ward, 1998) can the indeterminacy be overcome, which yields the mean first–passage times. The rate of spark generation in the limit $1 \ll N \ll \epsilon_m^{-\alpha}$ is (Hinch, 2004)

$$\tau_{\mathrm{gen}} \sim \left(\frac{e}{\sqrt{2\pi}}\right)^{\alpha-1} \frac{\tau_{\mathrm{open}} g(1/N)\sqrt{2\pi N}}{f(0)\sqrt{-\gamma_0 f(1/N) g(1/N)}} \exp\left(N \int_{1/N}^{\phi_0} \ln\left(\frac{g(\phi)}{f(\phi)}\right) \mathrm{d}\phi\right), \tag{10}$$

where ϕ_0 is the unstable fixed-point (i. e. $f(\phi_0) = g(\phi_0)$ and $f'(\phi_0) > g'(\phi_0)$); $\gamma_0 = g'(\phi_0)/g(\phi_0) - f'(\phi_0)/f(\phi_0)$; and τ_{open} is the dimensional mean open time of a RyR. Figure 4A shows the mean spark separation τ_{gen} as a function of myoplasmic $[\mathrm{Ca}^{2+}]$ for 3 different SR $[\mathrm{Ca}^{2+}]$. The points are the results of Monte Carlo simulations averaged over 1000 sparks and the lines are the asymptotic approximation (10). The quantities are plotted in dimensional units. Note that when the SR calcium is increased, the spark frequency increases dramatically. This has been observed in experiments where the frequency of Ca^{2+} sparks rapidly increases between waves as the SR Ca^{2+} store is slowly

replenished (Aptel and Freestone, 1998). In sections 3 and 4, the effect of stochasticity

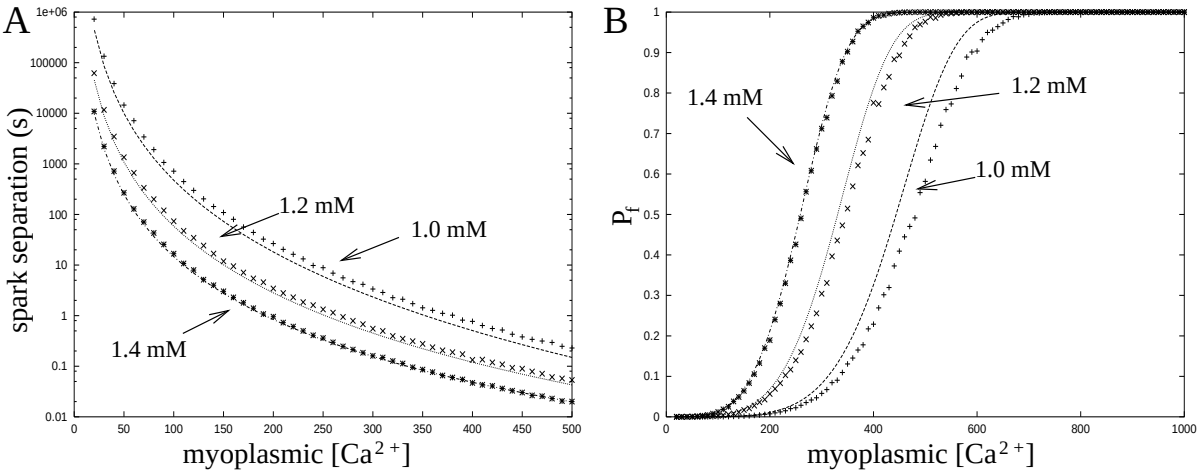

Fig. 4. A. The predicted spark separation for 3 different SR $[Ca^{2+}]$. The points were calculated using Monte Carlo simulations and the lines are using the asymptotic formula (10). Note that the time-scale is a log-scale. The non-dimensional parameter values are: $\alpha = 4$, $k = 0.2$, $\delta = 0.114$ $N = 40$, $\tau_{\rm open} = 0.5$ ms, $\epsilon_m = 0.1 \times [Ca^{2+}]_{\rm myo}$ and $J = 0.0035 \times [Ca^{2+}]_{\rm JSR}$ where the $[Ca^{2+}]$ are given in μM. B. The probability that a spark occurs in a sampling period of 50 ms. Note that these curves are approximately sigmoidal in shape.

on the propagation of Ca^{2+} waves will be investigated. For these sections it is necessary to calculate the probability (P_f) that a spark is generated in a set time interval τ as a function of $[Ca^{2+}]_{\rm myo}$. Assume $[Ca^{2+}]_{\rm myo}$ is constant during this interval so that the rate of spark generation is constant, then P_f can easily be calculated from (10) by

$$P_f = 1 - e^{-\tau/\tau_{\rm gen}}, \tag{11}$$

and is plotted in Figure 4B. Note that P_f has a sigmoidal shape as $[Ca^{2+}]_{\rm myo}$ is increased and the curve is shifted to the left as $[Ca^{2+}]_{\rm SR}$ is increased. The fact that P_f is a sigmoid function and not a step function is a stochastic effect. It is via P_f that the the stochastic nature of the individual channels influences the global pattern of Ca^{2+} release in the whole cell (section 3).

The second place stochasticity is observed in calcium sparks is in the variability of their duration. This has been observed both in experiments (Wang et al., 2002) and in computer simulations of spark models (Sobie et al., 2002). In both experiments (on a single release site) and models, the spark duration has a bell shaped distribution. We now show how the model of Ca^{2+} sparks can be analysed using stochastic phase–plane analysis to calculate

the distribution of spark durations (Hinch, 2002). Stochastic phase–plane analysis combines the theory of fixed–point stochastic transitions with the conventional phase–plane analysis of relaxation oscillators (e. g. FitzHugh-Nagumo type equations, see Keener and Sneyd (1998)). The spark model, (7) and (8), contains a fast-variable (ϕ) and a slow variable (J) since $\tau_{\mathrm{JSR}} \gg 1$. Consequently the system will remain in the regions of the stable null–clines (the fixed–points on the Markov chain) of $\phi(J)$. The null–clines of the spark model are shown in Figure 3B along with a sample solution in the phase–plane. At rest the system is at the fixed–point $\phi_- \approx 0$, which is [1] in Figure 3B. When a spark occurs, the system rapidly jumps to the null–cline $\phi_+(J)$ [2], and then moves down the null–cline as J slowly decreases according to

$$\tau_{\mathrm{JSR}} \frac{\mathrm{d}J}{\mathrm{d}t} = -J\phi_+(J) + r(J_0 - J). \tag{12}$$

In deterministic phase–plane analysis the system would remain in the region of $\phi_+(J)$ until it vanishes at [3] where the system jumps back to the null–cline $\phi_-(J)$. However, in the stochastic model there is the added possibility that the system undergoes a stochastic transition to $\phi_-(J)$ before [3] is reached. It is these stochastic transitions that lead to the bell–shaped distribution of spark durations. The rate of spark termination due to stochastic transitions can be calculated using the same technique used to calculate τ_{gen} (Hinch, 2004) and is

$$\kappa_{\mathrm{term}}(t) \sim \frac{f(\phi_+(J), J)\sqrt{-\gamma_0(J)\gamma_+(J)}}{2\pi N} \exp\left(N \int_{\phi_0(J)}^{\phi_+(J)} \ln\left(\frac{g(\phi, J)}{f(\phi, J)}\right) \mathrm{d}\phi\right), \tag{13}$$

where $J(t)$ is calculated using (12). The probability density of spark durations is then given by

$$p_{\mathrm{d}}(\tau) = \kappa_{\mathrm{term}}(\tau) \exp\left(-\int_0^\tau \kappa_{\mathrm{term}}(t)\, \mathrm{d}\tau\right). \tag{14}$$

The distribution of spark durations is plotted in Figure 5A. The line is the distribution calculated using stochastic phase–plane analysis and the bars are calculated using Monte Carlo simulations. The Monte Carlo simulation and the asymptotic analysis are only in a partial quantitative agreement, however in the limit $N, \tau_{\mathrm{JSR}} \to \infty$, the discrepancy between the numerical and asymptotic results tends to zero (data not shown). The model results are compared to experimental measurements (Figure 5B) of the distribution of spark rise (and therefore release) times from a hyperactive release site (Wang et al., 2002). The results of the model and the experiment are in reasonable agreement (it should be noted that this is a true model prediction since this experiment was not used to determine

the model parameters). The question of the mechanism of spark termination is still not

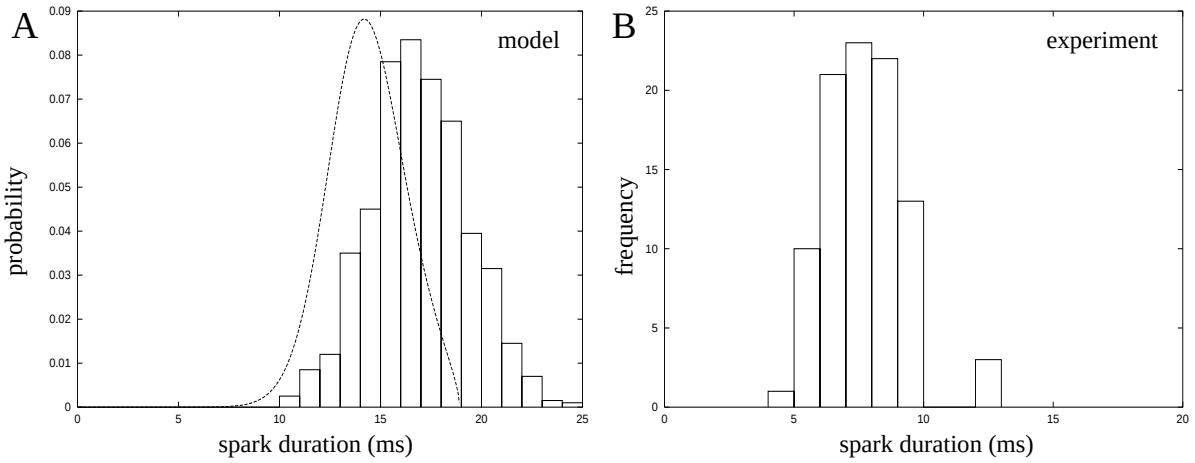

Fig. 5. A. The distribution of spark durations calculated using the model. The line is the calculation using stochastic phase–plane analysis and the bars are calculated using a Monte Carlo simulation. B. Experimental measurements of the spark rise time from a single hyperactive site (re-plotted from Wang et al. (2002)).

resolved. The mechanism used in this model is a partial depletion of JSR Ca^{2+} coupled with the RyRs being sensitive to JSR Ca^{2+}, which is consistent with the experimental findings of Terentyev et al. (2002). A recent result of Shannon et al. (2003) measuring stimulated Ca^{2+} release in cardiac myocytes has shown that the $[Ca^{2+}]$ in the NSR and JSR follow the same time-course, suggesting that there is no distinction between NSR and JSR. However, the time-scale over which this is measured is of the order of 200 ms, which does not imply that different $[Ca^{2+}]$ can occur on the shorter time-scale of 10 ms which is the duration of a spark.

In this section we analysed how the stochastic nature of single receptors affects the macroscopic behaviour of a whole CaRU. In the next section we shall investigate how the stochastic nature of CaRUs affects the propagation of Ca^{2+} waves.

3 Development of the FDF framework

Here we describe the idealised FDF model of Ca^{2+} release (Keizer et al., 1998) and its generalisation (Coombes and Timofeeva, 2003). In the FDF framework a site releases Ca^{2+} instantaneously (*fires*) when the value of $[Ca^{2+}]$ at the site exceeds some threshold value. The release events (Ca^{2+} *puffs* or *sparks*) lead to the propagation of travelling waves

via diffusion of Ca^{2+}. The partial differential equation describing the density of Ca^{2+} in the cytosol, denoted by $u(\mathbf{r},t)$, is given by

$$\frac{\partial u}{\partial t} = -\frac{u}{\tau_d} + D\nabla^2 u + \sum_{n\in\Gamma}\sum_{m\in\mathbb{Z}} \delta(\mathbf{r}-\mathbf{r}_n)\eta(t-T_n^m), \tag{15}$$

with $\mathbf{r}\in\mathbb{R}^l$ and $t\in\mathbb{R}^+$. Here l is the physical dimension of the cell model and Γ is a discrete set that indexes the stores. The vectors $\mathbf{r}_n$ determine the locations of the (point) Ca^{2+} release sites, whilst the T_n^m give the time of release of the mth release event (puff or spark) at the nth release site. The function $\eta(t)$ describes the shape of a Ca^{2+} release event which we shall take to have a rectangular pulse-shape given by

$$\eta(t) = \frac{\sigma}{\tau}\Theta(t)\Theta(\tau-t), \tag{16}$$

where Θ is a Heaviside step function. The strength of the calcium release event is σ and τ is interpreted as the rise-time of the receptor. The model is highly nonlinear because the release events are implicitly determined by the times at which the Ca^{2+} density at a release site takes on the threshold value u_c. More precisely we write

$$T_n^m = \inf\left\{t | u(\mathbf{r}_n,t) > u_c,\, u_t(\mathbf{r}_n,t) > 0,\, T_n^m > T_n^{m-1} + \tau_R\right\}, \tag{17}$$

to indicate that release events must be separated by at least a time τ_R, the refractory time-scale. The decay time τ_d in (15) models the time-scale associated with the action of SERCA pumps that re-sequester the Ca^{2+} back into the stores. The transport of Ca^{2+} is assumed to be by diffusion with diffusion coefficient D. For slow pumps ($\tau_d\to\infty$) and a regular array of release sites (with a lattice spacing d) the mode of propagation (continuous or saltatory) depends on the ratio of the time that a single site remains open to the time it takes for calcium to diffuse between neighbouring release sites (Pearson and Ponce Dawson, 1998; Ponce Dawson et al., 1999). If this ratio is large enough the propagation is continuous ($D\tau/d^2 \gg 1$), and wave speeds scale as $\sqrt{D}$, and if it is small enough the propagation is saltatory ($D\tau/d^2 \ll 1$), and wave speeds scale linearly with D. A more general discussion for arbitrary pump rates can be found in (Coombes, 2001). Importantly the FDF model reproduces the full range of wave propagation, from saltatory to continuous, whereas homogeneous reaction diffusion models predict only continuous propagation. This is shown in Figure 6 where a numerical simulation of the FDF model demonstrates the existence of continuous as well as saltatory Ca^{2+} signals. In panel A, the time constant for Ca^{2+} release is given by $\tau = 1$ s and the propagating signal is a smooth

travelling pulse. In panel B $\tau = 10$ μs and spark-like Ca^{2+} releases lead to a propagating signal that is distinctly saltatory. In this model the speed of the wave is determined by the time it takes Ca^{2+} released by the site at the front to diffuse to the next active site and raise the value of $[Ca^{2+}]$ there to the threshold.

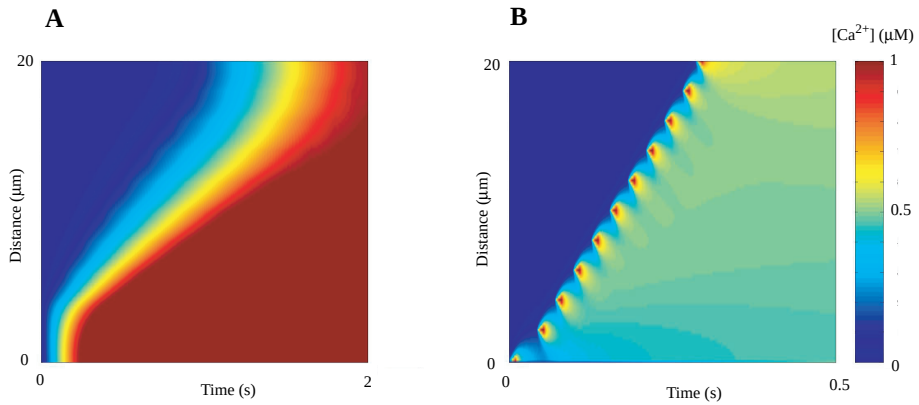

Fig. 6. Continuous (A) and saltatory (B) travelling wave propagations for the following parameters: $D = 30$ μm^2/s, $d = 2$ μm, $\sigma = 5$ μM$\cdot\mu$m, $u_c = 0.1$ μM and $\tau = 1$ s for panel A and 10 μs for panel B.

For a detailed discussion of the speed and stability of both continuous and saltatory waves in the FDF model see (Coombes, 2001; Timofeeva and Coombes, 2003). Making the reasonable assumption that release times occur at integer multiples of τ we may simplify the FDF model so that it can be re-written in the language of binary *release events*. We introduce a dynamics for the p*th* release event at the n*th* site using the binary variables $a_n(p) \in \{0, 1\}$, where

$$a_n(p) = \Theta(u_n(p) - u_c) \prod_{m=1}^{\min(R,p)} \Theta(u_c - u_n(p-m)). \tag{18}$$

Here $u_n(p) \equiv u(\mathbf{r}_n, p\tau)$ and $p, R \in \mathbb{Z}$. The first term on the right is a simple threshold condition for the determination of a release event whilst the second term ensures that release events are separated by at least $R\tau$, which we take to be the refractory time, i.e. $\tau_R = R\tau$. This restriction of the model eliminates the need for the precise (computationally expensive) determination of release times. The FDF model then takes the particularly simple form

$$Qu(\mathbf{r}, t) = \frac{\sigma}{\tau} \sum_{n \in \Gamma} a_n(p) \delta(\mathbf{r} - \mathbf{r}_n), \qquad p\tau < t < (p+1)\tau, \tag{19}$$

where Q is the linear differential operator

$$Q = \partial_t + \frac{1}{\tau_d} - D\nabla^2, \tag{20}$$

with Green's function

$$G(\mathbf{r}, t) = [4\pi D t]^{-l/2} \exp\left(-\frac{t}{\tau_d}\right) \exp\left(-\frac{r^2}{4Dt}\right), \tag{21}$$

and $r = |\mathbf{r}|$. The dynamics for $p\tau < t < (p+1)\tau$ is completely determined in terms of initial data $u_p(\mathbf{r}) = u(\mathbf{r}, p\tau)$ as

$$u(\mathbf{r}, t) = \frac{\sigma}{\tau} \sum_{n \in \Gamma} a_n(p) H(\mathbf{r} - \mathbf{r}_n, t - p\tau) + (G \otimes u_p)(\mathbf{r}, t), \tag{22}$$

where

$$H(\mathbf{r}, t) = \int_0^t G(\mathbf{r}, t - s)\, \mathrm{d}s, \tag{23}$$

and

$$(G \otimes u_p)(\mathbf{r}, t) = \int_{\mathbb{R}^l} G(\mathbf{r} - \mathbf{r}', t - p\tau) u_p(\mathbf{r}')\, \mathrm{d}\mathbf{r}'. \tag{24}$$

Release events defined by $a_n(p) = 1$ are easily calculated since $u_n(p) \equiv u_p(\mathbf{r}_n)$ may be written as a sum of two terms that are both amenable to fast numerical evaluation. In particular $u_p(\mathbf{r})$ may be written in terms of the *basis* functions $H_n(\mathbf{r}) = \sigma H(\mathbf{r} - \mathbf{r}_n, \tau)/\tau$, so that

$$u_p(\mathbf{r}) = \sum_{n \in \Gamma} a_n(p-1) H_n(\mathbf{r}) + (G \otimes u_{p-1})(\mathbf{r}, p\tau). \tag{25}$$

Since the basis functions $H_n(\mathbf{r})$ are fixed for all time they need only be computed once. For small τ we also have the useful result that $H(\mathbf{r}, \tau) \to G(\mathbf{r}, \tau)$, which is given in closed form by (21). Since the puff duration is very small compared to τ_R this is a very accurate approximation, and has been used in numerical simulations. The convolution in (25) may be performed efficiently using Fast Fourier Transform (FFT) techniques. Once again the FFT of $G(\mathbf{r}, \tau)$ need only be computed once, so that it is only necessary to successively construct the FFT of $u_p(\mathbf{r})$ for $p = 0, 1, 2, \ldots$. We then have that $G \otimes u_p = \mathcal{F}^{-1}(\mathcal{F}[G]\mathcal{F}[u_p])$, where $\mathcal{F}$ denotes the FFT. Hence, under the assumption that release times occur on some regular temporal lattice the model does not have to be evolved as a discontinuous partial differential equation with a self-consistent search for the times of threshold crossings that define release events. From experimental data it is apparent that the refractory time-scale is typically 50 times that of the release duration so we assume $R = 50$ in our simulations if it is not specified. Typically τ is approximately $10 - 100$ms.

Most of the theoretical work on calcium signalling has focused on deterministic models of intracellular Ca^{2+} waves. Only relatively recently has the stochastic nature of intracellular Ca^{2+} release been considered (Keizer and Smith, 1998; Falcke et al., 2000; Falcke, 2003; Shuai and Jung, 2002a,b). Here we describe a stochastic generalisation of the FDF threshold model which uses a probabilistic rather than a deterministic update rule. The analysis of the spark model (section 2) showed the probability of a spark in a time period τ is a sigmoidal shape with intracellular Ca^{2+} (see Figure 4B). Taking this as a generic model for a CaRU suggests that a natural way to determine the probability of a release event (i.e. the probability that $a_n(p) = 1$) is to generalise (18) and write

$$P(a_n(p) = 1) = P_f(u_n(p)) \prod_{m=1}^{\min(R,p)} \Big(1 - P_f(u_n(p-m))\Big), \tag{26}$$

where P_f is given by (11). For convenience we write

$$P_f(u) = \Psi(u - u_c), \tag{27}$$

where the threshold concentration u_c is given by $P_f(u_c) = 1/2$. For simplicity we approximate Ψ with a one-parameter family of sigmoids

$$\Psi(u) = \left\{ \frac{1}{1 + \mathrm{e}^{-\beta u}} - \frac{1}{1 + \mathrm{e}^{\beta u_c}} \right\} (1 + \mathrm{e}^{-\beta u_c}), \tag{28}$$

such that the probability of release is zero when $u = 0$ and tends to one as $u \to \infty$. In summary, the stochastic FDF model is defined by the equation (22) with the $a_n(p) \in \{0, 1\}$ treated as random variables such that $P(a = 1)$ is given by (26). Note, that in the limit $\beta \to \infty$, this function approaches a step function so that $P_f(u) = \Theta(u - u_c)$ and we recover our original deterministic model. Thus we interpret β as a parameter giving an indirect measure of the cluster size and thus the level of noise. In the stochastic FDF framework the refractory time-scale can also be thought of as being drawn from some distribution, since release events are no longer bound by the constraint that they be separated by at least τ_R.

4 Rhythms and waves

The best way to illustrate the sort of behaviours that can be generated by the computationally inexpensive stochastic FDF model is by a space-time density plot for calcium concentration. In real cells release sites are never quite arranged on a perfectly regular

lattice. In our simulations we give examples of both regular and disordered distributions of release sites (assuming free boundary conditions so that wave propagation in the system is restricted only by cell size). First of all, we present simulation results on a regular lattice of release sites in one dimension, with lattice spacing d, without receptor noise. In Figure 7 we show a solitary lurching pulse arising from an initially activated release site in the middle of the cell. This nicely illustrates that a discrete set of release sites leads to a wave that propagates with a non-constant profile, but with a well defined speed.

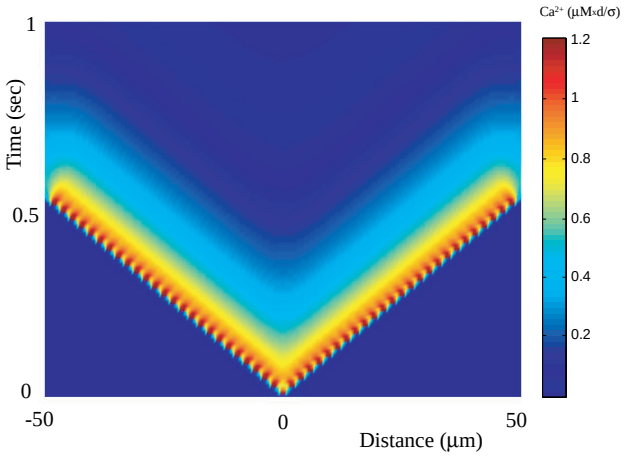

Fig. 7. An example of two lurching pulses moving out from the center of a deterministic one dimensional FDF model with 50 regularly spaced release sites and free boundary conditions. Parameters: $d = 2\mu$m, $D = 30\mu\text{m}^2/\text{s}$, $\tau = 10$ms, $\tau_d = 0.2\mu\text{M/s}$, $u_c = 0.1$ for a cell of linear dimension 100μm.

Next, in Figure 8 we show an example of behaviour in the deterministic two-dimensional FDF model with an initially active single release site in the center of the cell model. Here a sequence of snap shots shows nucleation of a wave front and subsequent propagation of the wave through the cell. Repetitive nucleation occurs in the middle of the cell with the period between successive waves largely determined by the refractory time-scale. Note that the octagonal shape of the wave front (rather than a circular one) is due to the underlying square array of release sites.

Different choices of initial condition give rise to more complex patterns of wave propagation. For example, in Figure 9 we show how a spiral wave may be initiated from a line of active release sites.

Now we consider a disordered distribution of release sites in two dimensions, such that a regular square array of release sites is perturbed by a small random vector. Comparing

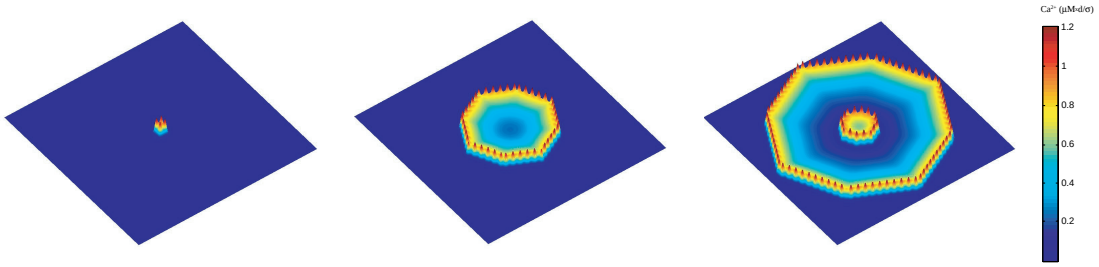

Fig. 8. Temporal sequence snapshots for the deterministic two-dimensional FDF model of size $120\mu m \times 120\mu m$ with release sites arranged on a regular square lattice (with spacing 2μm). Other parameters as in Figure 7. Frames are presented every 0.29 s starting from the left. An initial seed in the center of the cell model leads to the formation and propagation of a well defined wave front. After approximately a refractory time period a new release event appears in the middle of the cell giving rise to a new propagating front of activity.

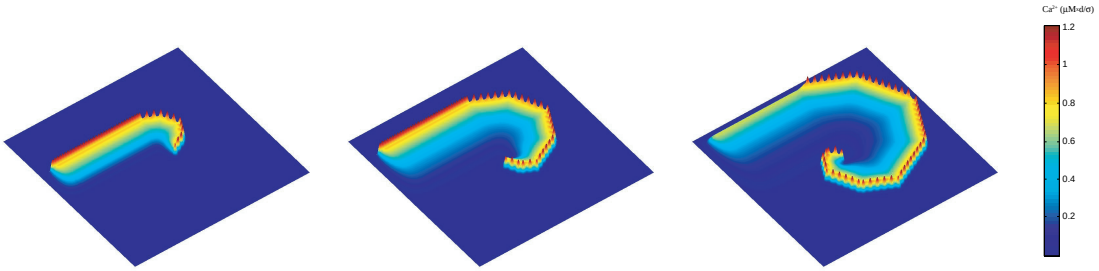

Fig. 9. Initiation of a spiral wave in the two-dimensional FDF model via activation of a line of release sites. Parameters as in Figure 8.

Figure 10 to Figure 8, the irregularity of the release sites causes the propagation of more circular wave fronts with unequal activities. Increasing the amount of spatial disorder ultimately leads to propagation failure.

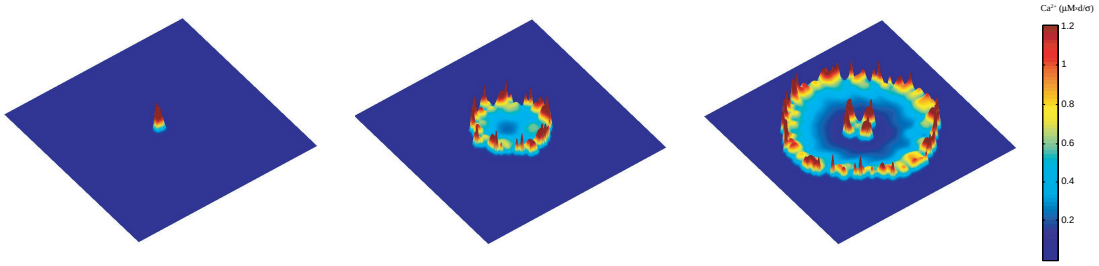

Fig. 10. Temporal sequence snapshots for the deterministic two-dimensional FDF model of size $120\mu m \times 120\mu m$ with release sites perturbed in random directions by an amount $0.4d$ from a regular square lattice. Other parameters as in Figure 8.

Next we illustrate the sort of behaviours that can be generated in the presence of receptor noise. In Figure 11 we plot the corresponding behaviour to Figure 7 in the presence of a finite amount of noise. Initial release from the central site leads to a local elevation of Ca^{2+} which initiates a propagating Ca^{2+} wave via activation of nearby sites, as in the deterministic case. However, the stochastic nature of the wave is evident from the fact that it does not propagate symmetrically away from the initial event. Although rather well defined to start with the leftward propagating wave terminates at around 1.4 s. This type of behaviour is observed in experimental linescan images of Ca^{2+} waves (Figure 1C). Activity in the wake of the primary stochastic wave can also be sufficient to *prime* release sites for subsequent spark production, seen at around 1.6 s and again at around 3.2 s.

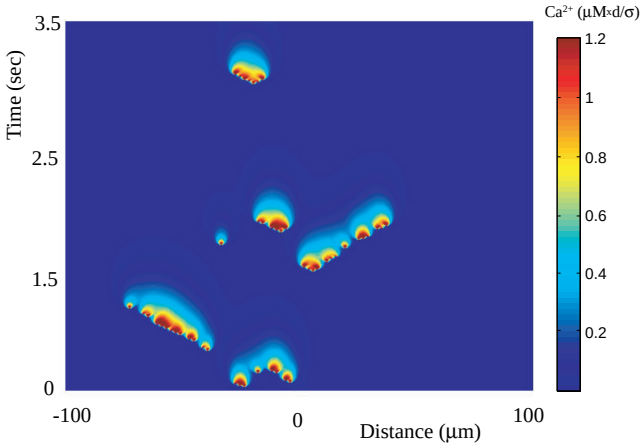

Fig. 11. Stochastic travelling wave for the model of Figure 7 with a finite amount of noise. Here $\beta = 10$.

In Figure 12 we show the effects of receptor noise in a two-dimensional cell with a regular square array of release sites.

The sequence of snap shots shows nucleation of a circular front, subsequent propagation and the emergence of noisy spiral waves. These waves can be annihilated in collisions with other waves and created by spontaneous nucleation. The long time behaviour of the system is dominated by the interaction of irregular target and spiral waves. This is typical of dynamics in noisy spatially extended excitable systems (Jung and Mayer-Kress, 1995b,a). Since noise sustained target waves may collide with each other this typically limits their growth to a finite region, whose size is expected to decrease with increasing noise. For increasing noise it is possible that the breakup of spirals and increased spontaneous nucleation of other spirals may destroy any coherent motion. In common with more biophysically detailed, yet computationally intensive models, stochastic calcium release

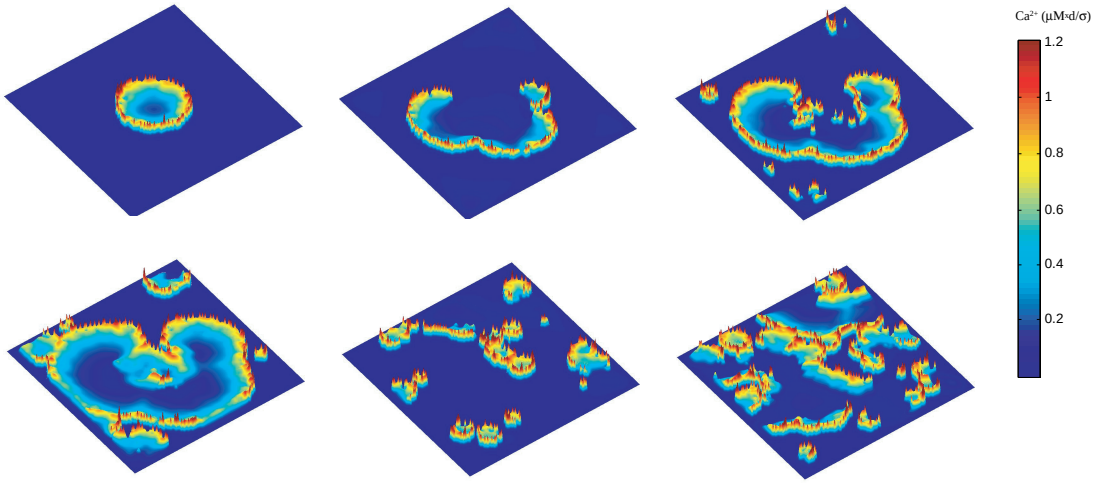

Fig. 12. Temporal sequence snapshots for the two-dimensional stochastic FDF model with $\beta = 100$ (low noise). Other parameters as in Fig. 8. Frames are presented every 0.18 s starting in the top left corner and moving rightward and down. An initial seed in the center of the cell model leads to the formation and propagation of a circular front. Spiral waves form in the wake of the wave by spontaneous nucleation. These can be destroyed in wave-wave collisions and created by spontaneous nucleation.

leads to the spontaneous production of calcium sparks that may merge to form saltatory waves. Moreover, sufficiently large noise is able to terminate a wave prematurely suggesting that for some critical noise level there is a non-equilibrium phase transition between propagating and abortive waves. A statistical analysis shows that the model exhibits properties consistent with behaviour of other models from the universality class of directed percolation (see (Coombes and Timofeeva, 2003) for further discussion).

However, it is also possible to see coherent motion for high levels of noise. In fact coherence can actually be enhanced in regions of high noise and it is possible to observe synchronised global release events. This type of behaviour has recently been termed *array enhanced coherence resonance* (AECR) and is typical of the way in which noise can lead to structured activity in spatially extended excitable systems (Hempel et al., 1999; Hu and Zhou, 2000; Zhou et al., 2001). In Figure 13 we show an example of this type of phenomenon in the stochastic FDF model, for a regular square array of release sites.

Here an initial disturbance leads to the propagation of a circular target wave. In the wake of the wave there is then subsequent release from a set of neighbouring sites. After this one sees near simultaneous release from a large number of sites. This process of simultaneous

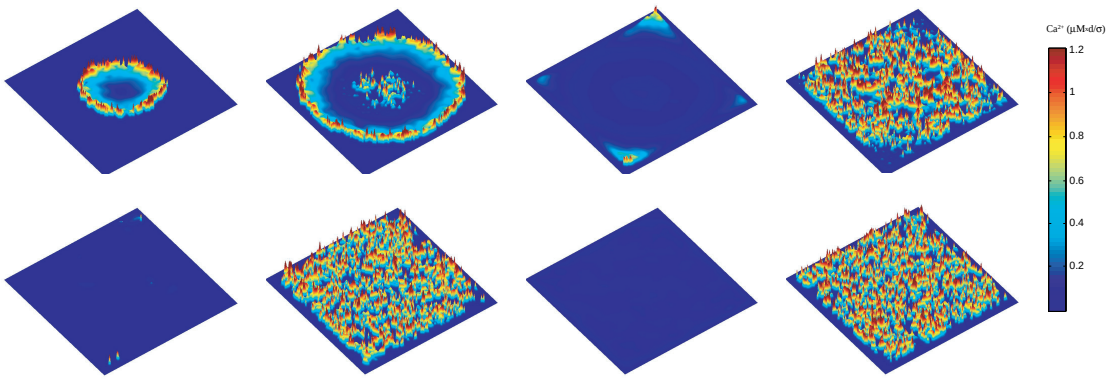

Fig. 13. Temporal sequence snapshots for the two-dimensional stochastic FDF model with $\beta = 10$ (high noise). Other parameters as in Figure 8. Frames are presented every 0.45 s starting in the top left corner and moving rightward and down. An initial seed leads to the formation of a circular travelling front. In the wake of the wave there is periodic and near simultaneous release from a large number of stores, typical of systems exhibiting array enhanced coherence resonance.

release repeats and at every stage recruits more and more stores. After only a few cycles of this process one sees an almost simultaneous release from all sites. The frequency of the AECR oscillation increases monotonically with the noise level β^{-1} (above a cut-off below which AECR fails). We emphasize that the coherent motion illustrated in Figure 13 is induced purely by noise without an external periodic signal. In this example a removal of all noise would lead to a deterministic system which could not support travelling waves. For further discussion of AECR in the stochastic FDF model see (Coombes and Timofeeva, 2003). The role of noise induced coherence in cell signalling is an important and growing area of study, as exemplified by the recent work of Shuai and Jung (2003). These authors have used a stochastic model of an IP_3 receptor to explore the role of channel clustering in generating AECR. One novel prediction of this work is that real cells may exploit an optimal channel clustering strategy to enhance the cellular response to weak stimulation.

5 Discussion

In this paper we have presented an integrative multi-scale framework to study the stochastic nature of Ca^{2+} release in cells. An asymptotic analysis was used to show how the Markov properties of individual receptors on the sub-millisecond time-scale effect the behaviour of a cluster of receptors on a much longer time-scale (section 2). Integrating

between these time-scales allowed us to develop a computationally efficient scheme to calculate the behaviour of a spatially extended cell model (sections 3 and 4). This approach allowed us to examine behaviour which can only be observed in stochastic systems, and in particular AECR. This phenomenon could play a potentially important role in the development of ectopic beats in the heart. For an intracellular Ca^{2+} oscillation to trigger an ectopic beat it is necessary that it first triggers an action potential. This can only be triggered if the sodium–calcium exchange (NCX) current associated with a Ca^{2+} oscillation is sufficiently large and rapid. However, in experiments on isolated myocytes, Ca^{2+} waves rarely trigger an action potential. If Ca^{2+} release was simultaneous throughout the cell (i. e. if the Ca^{2+} oscillations were due to AECR) rather than in the form of a wave, the induced NCX current would have a larger amplitude, increasing the likelihood of an action potential being evoked.

Apart from being directly relevant to cardiac myocytes, the framework that we have presented for studying intracellular calcium waves is a general one that can handle many cell types. Although for clarity of exposition we have focused on cells that express RyRs it is also possible to follow through the program of reduction we have described for other receptor models. In particular the high dimensional model of an IP_3 receptor due to De Young and Keizer (1992) has recently been reduced to a simple state and parameter dependent FDF threshold (Timofeeva and Coombes, 2003). Importantly, by building upon early theoretical insights gained from the study of fire-diffuse-fire models we have begun to uncover how noise and heterogeneity can contribute to calcium signalling in spatially extended cells with discrete release sites. The recent experimental progress in determining the precise spatio-temporal recruitment pattern of sparks in rat atrial myocytes (Mackenzie et al., 2001) provides an ideal testing ground for the use of a stochastic FDF framework to understand the behaviour of real cells. An important aspect of this particular cell that can naturally be accommodated within our FDF framework is the separation of stores into subsarcolemmal junctional SR (JSR) and central nonjunctional SR (NJSR) classes. It is known that Ca^{2+} rise in atrial myocytes occurs at so-called *eager-sites* in the subsarcolemmal region followed by CICR wave propagation into the deeper layers of the cell. It would appear that enhanced excitability of the eager-sites leads to a predetermined microscopic activation sequence of Ca^{2+} sparks whereby single cells produce reproducible inhomogeneous Ca^{2+} release upon depolarisation. Models of the VOCC channels (that mediate the entry of the electrical signal into the cell) may be developed using an appropriate FDF voltage dependent (rather than Ca^{2+}) threshold function. Since eager-sites display

the highest frequency of spontaneous Ca^{2+} sparks in resting cells the functional distinction between JSR and NJSR stores may be modelled using a non-uniform distribution of thresholds. In particular the use of a stochastic FDF model will allow the investigation of how the geometry of release sites gives rise to nucleation phenomena. Furthermore, such a modelling study will be able to probe the way in which the failure to recruit Ca^{2+} sparks appropriately can lead to defective excitation-contraction coupling in cardiac cells (Gomez et al., 1997). The results of this more detailed study will be presented elsewhere.

Acknowledgements

SC would like to acknowledge support from the UK Royal Society. RH would like to acknowledge support from the British Heart Foundation and The Wellcome Trust; Prof D Noble and Dr A Fowler who supervised his DPhil during which much of the work in section 2 was done; and Prof D Eisner and Dr SC O'Neill of the University of Manchester in whose laboratory the experimental Ca^{2+} images were recorded.

References

N Allbritton and T Meyer. Localized calcium spikes and propagating calcium waves. *Cell Calcium*, 14:691–697, 1993.

H Aptel and N Freestone. Correlation between Ca^{2+} waves, Ca^{2+} sparks and the loading of the SR in rat ventricular cardiomyocytes. *Journal of Physiology*, 509P:155P, 1998.

M J Berridge. Elementary and global aspects of calcium signalling. *Journal of Neurophysiology*, 499:291–306, 1997.

M D Bootman, P Lipp, and M J Berridge. The organisation and function of local Ca^{2+} signals. *Journal of Cell Science*, 114:2213–2222, 2001.

N Callamaras, J S Marchant, X P Sun, and I Parker. Activation and co-ordination of InsP(3)-mediated elementary Ca^{2+} events during global Ca^{2+} signals in Xenopus oocytes. *Journal of Physiology*, 509:81–91, 1998.

H Cheng, W J Lederer, and M B Cannell. Calcium sparks - elementary events underlying excitation-contraction coupling in heart muscle. *Science*, 262:740–744, 1993.

S Coombes. The effect of ion pumps on the speed of travelling waves in the fire-diffuse-fire model of Ca^{2+} release. *Bulletin of Mathematical Biology*, 63:1–20, 2001.

S Coombes and Y Timofeeva. Sparks and waves in a stochastic fire-diffuse-fire model of Ca^{2+} release. *Physical Review E*, 68:021915, 2003.

G W De Young and J Keizer. A single pool IP_3-receptor based model for agonist stimulated Ca^{2+} oscillations. *Proceedings of the National Academy of Sciences USA*, 89: 9895–9899, 1992.

M Falcke. On the role of stochastic channel behaviour in intracellular Ca^{2+} dynamics. *Biophysical Journal*, 84:42–56, 2003.

M Falcke, L Tsimring, and H Levine. Stochastic spreading of intracellular Ca^{2+} release. *Physical Review E*, 62:2636–2643, 2000.

R A Fontanilla and R Nuccitelli. Characterization of the sperm-induced calcium wave in Xenopus eggs using confocal microscopy. *Biophysical Journal*, 75:2079–2087, 1998.

A M Gomez, H H Valdivia, H Cheng, M R Lederer, L F Santana, M B Cannell, S A McCune, R A Altschuld, and W J Lederer. Defective excitation-contraction coupling in experimental cardiac hypertrophy and heart failure. *Science*, 276:800–806, 1997.

S Gyorke and M Fill. Ryanodine receptor adaptation: control mechanism of Ca^{2+} induced Ca^{2+} release in the heart. *Science*, 260:807–809, 1993.

H Hempel, L Schimansky-Geier, and J Garcia-Ojalvo. Noise-sustained pulsating patterns and global oscillations in subexcitable media. *Physical Review Letters*, 82:3713–3716, 1999.

R Hinch. *Mathematical models of the heart.* PhD thesis, Oxford University, UK., 2002.

R Hinch. A mathematical analysis of the generation and termination of calcium sparks. *Biophysical Journal*, 86(3), 2004.

B Hu and C Zhou. Phase synchronization in coupled nonidentical excitable systems and array-enhanced coherence resonance. *Physical Review E*, 61:R1001–R1004, 2000.

P Jung and G Mayer-Kress. Noise controlled spiral growth in excitable media. *Chaos*, 8: 458–462, 1995a.

P Jung and G Mayer-Kress. Spatiotemporal stochastic resonance in excitable media. *Physical Review Letters*, 74:2130–2133, 1995b.

J Keener and J Sneyd. *Mathematical Physiology.* Springer, 1998.

J E Keizer and G D Smith. Spark-to-wave transition: saltatory transmission of calcium waves in cardiac myocytes. *Biophysical Chemistry*, 72:87–100, 1998.

J E Keizer, G D Smith, S Ponce Dawson, and J Pearson. Saltatory propagation of Ca^{2+} waves by Ca^{2+} sparks. *Biophysical Journal*, 75:595–600, 1998.

V Lukyanenko, T F Wiesner, and S Gyorke. Termination of Ca^{2+} release during Ca^{2+}

sparks in rat ventricular myocytes. *Journal of Physiology*, 507:667–677, 1998.

L Mackenzie, M D Bootman, M J Berridge, and P Lipp. Predetermined recruitment of calcium release sites underlies excitation-contraction coupling in rat atrial myocytes. *Journal of Physiology*, 530:417–429, 2001.

R Nuccitelli, D L Yim, and T Smart. The sperm- induced Ca^{2+} wave following fertilization of the Xenopus eggs requires the production of Ins(1,4,5)P3. *Developmental Biology*, 158:200–212, 1993.

I Parker, J Choi, and Y Yao. Elementary events of InsP3-induced Ca^{2+} liberation in Xenopus oocytes: hot spots, puffs and blips. *Cell calcium*, 20:105–121, 1996.

I Parker and Y Yao. Regenerative release of calcium from functionally discrete subcellular stores by inisitol trisphosphate. *Proceedings of the Royal Society London B*, 246:269–274, 1991.

J E Pearson and S Ponce Dawson. Crisis on skid row. *Physica A*, 257:141–148, 1998.

S Ponce Dawson, J Keizer, and J E Pearson. Fire-diffuse-fire model of dynamics of intracellular calcium waves. *Proceedings of the National Academy of Sciences USA*, 96: 6060–6063, 1999.

T S Shannon, T Guo, and D M Bers. Ca^{2+} scraps: Local deplation of free [Ca^{2+}] in cardiac sarcoplasmic reticulum during contractions leave substantial Ca^{2+} reserve. *Cirulatory Research*, 93:40–45, 2003.

J W Shuai and P Jung. Optimal intracellular calcium signalling. *Physical Review Letters*, 88:068102, 2002a.

J W Shuai and P Jung. Stochastic properties of Ca^{2+} release of inositol 1,4,5-trisphosphate receptor clusters. *Biophysical Journal*, 83:87–97, 2002b.

J W Shuai and P Jung. Optimal ion channel clustering for intracellular calcium signalling. *Proceedings of the National Academy of Science USA*, 100:506–510, 2003.

J Sneyd. *An introduction to Mathematical Modeling in Physiology, Cell Biology, and Immunology*, chapter Calcium excitability, pages 83–118. American Mathematical Society, 2002.

E A Sobie, K W Dilly, J dos Santos Cruz, W J Lederer, and M S Jafri. Termination of Ca^{2+} sparks: An investigative mathematical mode of Ca^{2+} induced Ca^{2+} release in the cardiac diad. *Biophysical Journal*, 83:59–78, 2002.

M D Stern. Theory of excitation–coupling in cardiac muscle. *Biophyscial Journal*, 63: 469–489, 1992.

D Terentyev, S Viatchenko-Karpinski, H H Valdivia, A L Escobar, and S Gyorke. Lumi-

nal Ca^{2+} controls termination and refractory behaviour of Ca^{2+} induced Ca^{2+} release in cardiac myocytes. *Cirulatory Research*, 91:414–420, 2002.

S E Thedford, W J Lederer, and H H Valdivia. Activation of SR Ca^{2+} release channels by intraluminal Ca^{2+}. *Biophysical Journal*, 66:A20, 1994.

Y Timofeeva and S Coombes. Wave bifurcation and propagation failure in a model of calcium release. *Journal of Mathematical Biology*, 47:249–269, 2003.

S Q Wang, L S Long, L Xu, G Meissner, E Lakatta, E Rios, M D Stern, and H Cheng. Thermodynamically irreversible gating of RyRs in situ revealed by stereotyped duration of release of Ca^{2+} sparks. *Biophysical Journal*, 83:242–251, 2002.

M J Ward. *Analysing multiscale phenomena using singular perturbation methods*, volume 56 of *Proceedings of Symposia in Applied Mathematics*, chapter Exponential asymptotics and convection–diffusion–reactions models, pages 151–184. AMS Short Courses, 1998.

Y Yao, J Choi, and I Parker. Quantal puffs of intracellular Ca^{2+} evoked by inositol trisphosphate in Xenopus oocytes. *Journal of Physiology*, 482:533–553, 1995.

A Zahradnikova and I Zahradnik. A minimal gating model for the cardiac Ca^{2+} release channel. *Biophysical Journal*, 71:2996–3012, 1996.

C Zhou, J Kurths, and B Hu. Array-enhanced coherence resonance: nontrivial effects of heterogeneity and spatial independence of noise. *Physical Review Letters*, 87:098101, 2001.